



ARTICLE OPEN

Quinpirole ameliorates nigral dopaminergic neuron damage in Parkinson's disease mouse model through activating GHS-R1a/D₂R heterodimers

Ting-ting Tang¹, Ming-xia Bi¹, Mei-ning Diao¹, Xiao-yi Zhang¹, Ling Chen¹, Xue Xiao¹, Qian Jiao¹, Xi Chen¹, Chun-ling Yan¹, Xi-xun Du¹✉ and Hong Jiang^{1,2}✉

Growth hormone secretagogue receptor 1a (GHS-R1a) is an important G protein-coupled receptor (GPCR) that regulates a variety of functions by binding to ghrelin. It has been shown that the dimerization of GHS-R1a with other receptors also affects ingestion, energy metabolism, learning and memory. Dopamine type 2 receptor (D₂R) is a GPCR mainly distributed in the ventral tegmental area (VTA), substantia nigra (SN), striatum and other brain regions. In this study we investigated the existence and function of GHS-R1a/D₂R heterodimers in nigral dopaminergic neurons in Parkinson's disease (PD) models in vitro and in vivo. By conducting immunofluorescence staining, FRET and BRET analyses, we confirmed that GHS-R1a and D₂R could form heterodimers in PC-12 cells and in the nigral dopaminergic neurons of wild-type mice. This process was inhibited by MPP⁺ or MPTP treatment. Application of QNP (10 μM) alone significantly increased the viability of MPP⁺-treated PC-12 cells, and administration of quinpirole (QNP, 1 mg/kg, i.p. once before and twice after MPTP injection) significantly alleviated motor deficits in MPTP-induced PD mice model; the beneficial effects of QNP were abolished by GHS-R1a knockdown. We revealed that the GHS-R1a/D₂R heterodimers could increase the protein levels of tyrosine hydroxylase in the SN of MPTP-induced PD mice model through the cAMP response element binding protein (CREB) signaling pathway, ultimately promoting dopamine synthesis and release. These results demonstrate a protective role for GHS-R1a/D₂R heterodimers in dopaminergic neurons, providing evidence for the involvement of GHS-R1a in PD pathogenesis independent of ghrelin.

Keywords: Parkinson's disease; growth hormone secretagogue receptor 1a; dopamine type 2 receptor; heterodimers; quinpirole; CREB signaling pathway

Acta Pharmacologica Sinica (2023) 44:1564–1575; <https://doi.org/10.1038/s41401-023-01063-0>

INTRODUCTION

Parkinson's disease (PD) is a chronic disease of the central nervous system that affects the mobility of patients. It mostly occurs in middle-aged and elderly people [1, 2]. The main pathological changes are the loss of dopaminergic neurons in the substantia nigra pars compacta, which further reduces the release of dopamine (DA) in the striatum and leads to movement disorders [3, 4]. Growth hormone secretagogue receptor 1a (GHS-R1a) is a typical G-protein-coupled receptor (GPCR) that is widely distributed in the hippocampus, substantia nigra (SN), hypothalamus, pituitary and ventral tegmental area (VTA) [5, 6]. In our previous study, GHS-R1a was found to increase the excitability of nigral dopaminergic neurons by inhibiting voltage-gated potassium channels through the activation of the PLC-PKC pathway [7]. A study also demonstrated that motor coordination dysfunction could be observed when a selective GHS-R1a antagonist was stereotactically injected into the SN of normal control mice [8]. Downregulation of GHS-R1a could also lead to motor coordination dysfunction [8] and mood disorders [9]. Conversely, a GHS-R1a agonist was found to mitigate behavioral dysfunction in

spontaneously hyperactive mice and cocaine-exposed mice, thereby modulating abnormal DA-mediated behavior [10].

In addition, there is growing evidence that GHS-R1a can participate in a variety of physiological activities in vivo by forming heterodimers with other receptors in the absence of ghrelin, exerting a ligand-independent constitutive effect [11–15]. In the periphery, GHS-R1a can form heterodimers with melanocortin 3 receptor [16, 17], 5-hydroxytryptamine 2c receptor [18, 19], orexin 1 receptor [20, 21] and G protein-coupled receptor 83 [22] to regulate food intake and energy metabolism. In the dentate gyrus of the hippocampus, GHS-R1a can form heterodimers with dopamine type 1 receptor (D₁R) to regulate synaptic plasticity through activation of the Gαq-PLC-IP3-Ca²⁺ pathway by a D1R agonist [23]. Dopamine type 2 receptor (D₂R) is a GPCR with seven transmembrane domains [24, 25] that is mainly distributed in the SN, nucleus accumbens, striatum, VTA, olfactory tubercle and hypothalamus [26]. Previous studies showed that D₂R^{-/-} rats exhibited PD-like behavioral impairment, such as spontaneous motor dysfunction [27], decreased motion initiation frequency [27] and spontaneous muscle tone [28] and impaired motor skill

¹Department of Physiology, Shandong Provincial Key Laboratory of Pathogenesis and Prevention of Neurological Disorders and State Key Disciplines: Physiology, School of Basic Medicine, Qingdao University, Qingdao 266021, China and ²University of Health and Rehabilitation Sciences, Qingdao 266000, China
Correspondence: Xi-xun Du (xunxundu@qdu.edu.cn) or Hong Jiang (hongjiang@qdu.edu.cn)

Received: 1 November 2022 Accepted: 12 February 2023

Published online: 10 March 2023

learning [27]. Given the roles of GHS-R1a and D₂R in regulating the function of dopaminergic neurons, it is of vital importance to clarify whether endogenous GHS-R1a and D₂R could form heterodimers in the SN and the role of these heterodimers in dopaminergic neurons in PD.

cAMP response element binding protein (CREB) is a broad transcriptional regulatory factor that regulates the expression of brain-derived neurotrophic factor, activating transcription factor-3, transcription 3, c-Fos, cAMP response element modulator, cyclin A and other genes [29–34]. It plays an important role in synaptic plasticity, learning and memory, and neuronal development [34–38]. CREB can be phosphorylated upstream of Ca²⁺/calmodulin (CaM) [39], promoting the growth of dorsal root ganglion neurons by upregulating brain-derived neurotrophic factor [40] and alleviating the symptoms of Alzheimer's disease in mice [41]. As two key factors in the synthesis and release of DA [42–45], tyrosine hydroxylase (TH) and vesicle monoamine transporter 2 (VMAT2) are both downstream targets of CREB [46–48]. In addition, the activity of CaM protein is decreased in 1-methyl-4-phenyl-1,2,3,6-tetrahydropyridine (MPTP)-induced PD mice model, resulting in cognitive deficits and learning disabilities [49, 50]. However, it is not clear whether the activation of GHS-R1a/D₂R heterodimers affects the expression of TH and VMAT2 via CREB phosphorylation, thus regulating DA synthesis and metabolism.

In the present study, the existence of GHS-R1a/D₂R heterodimers was confirmed in dopaminergic cells and neurons. Using MPTP-induced PD mice model, we aimed to investigate whether activation of the GHS-R1a/D₂R heterodimers affects the synthesis and release of DA. To explore the underlying mechanism, we assessed the protein levels of CaM, CREB and downstream targets of TH and VMAT2. We aimed to elucidate the potential molecular mechanisms of GHS-R1a/D₂R heterodimers on PD pathogenesis to provide a new drug target for PD treatment.

MATERIALS AND METHODS

Animals and treatment

GHS-R1a knockout (*Ghsr*^{-/-}) mice were ordered from the Shanghai Model Organisms Center. Male *Ghsr*^{-/-} mice and their littermate wild-type (WT) mice were used in this experiment. Fifteen to sixteen-week-old mice weighing (25 ± 2) g were housed on a 12 h light/dark cycle at a room temperature of (22 ± 2) °C to mimic natural conditions. The mice were given food and purified water ad libitum. Animal experiments were carried out according to the National Institutes of Health Guidelines for the Care and Use of Laboratory Animals. All protocols were approved by the Animal Ethics Committee of Qingdao University.

Adult mice were intraperitoneally injected with 0.5 or 1 mg/kg quinpirole (QNP) (TOCRIS). Behavioral tests were performed at 0.5, 1, 2, 4 and 6 h after injection, and brain tissues were collected. Then, the microdialysis experiment was carried out first, and 1 day after recovery, *Ghsr*^{-/-} and WT mice were intraperitoneally injected with 1 mg/kg QNP or normal saline (NS), 4 h before MPTP (Sigma) injection (Fig. 4a). Then, MPTP (20 mg/kg) was intraperitoneally injected 4 times at an interval of 2 h for acute MPTP treatment. Finally, the mice were injected with QNP (1 mg/kg) twice at an interval of 4 h. On the fourth and fifth days, the mice were subjected to behavioral tests and a microdialysis study. The animals were sacrificed, and their brains were harvested on the sixth day.

Cell culture and transfection

PC-12 cells were purchased from the National Infrastructure of Cell Line Resource (Shanghai, China) and cultured in RPMI-1640 medium with 10% fetal bovine serum (TransGen Biotech, China) and 1% penicillin–streptomycin at 37 °C in 5% CO₂. Cell transfection was performed by Lipofectamine 2000 (Invitrogen, USA) reagent according to the manufacturer's protocol.

Plasmids and viruses

PC-12 cells were transfected with the pcDNA3.1-D₂R, pcDNA3.1-GHS-R1a, or pcDNA3.1-D₂R/pcDNA3.1-GHS-R1a plasmid. The D₂R and GHS-R1a plasmids were purchased from OBiO Technology (Shanghai, China). To establish stable cell lines, PC-12 cells were transfected with shRNA-GHS-R1a, which was purchased from OBiO Technology (Shanghai, China).

Immunofluorescence staining

Brain tissues were trimmed, and tissues containing the substantia nigra pars compacta were sectioned into 20 μm slices (Leica, Germany). Fifty frozen sections from each mouse were divided into four sets. One set was randomly selected for immunofluorescence staining to observe the colocalization of GHS-R1a and D₂R. Brain slices and cells were blocked with 10% goat serum and incubated with mouse anti-GHS-R1a (Absin, 1:50) and rabbit anti-D₂R (Santa Cruz, 1:50) overnight at 4 °C. The cells or tissues were then washed with PBS and incubated with Alexa Fluor® 555-conjugated goat anti-mouse IgG (H + L) (1:500), Alexa Fluor® 488-conjugated goat anti-rabbit IgG (H + L) (1:500) and Alexa Fluor® 555-conjugated goat anti-rabbit IgG (H + L) (1:500) secondary antibodies for 1 h at room temperature, and DAPI was added for 5 min before mounting with antifade solution. Images were acquired using immunofluorescence microscopy (Leica, Germany).

Western blotting

The SN was precisely dissected out, and the tissues were incubated with RIPA lysis buffer (CWBI, China) containing protease inhibitors and lysed for 30 min on ice after being fully ground. After centrifugation at 12,000 rpm for 20 min at 4 °C, the supernatant was removed for determination of the protein concentration by a Bradford assay kit (CWBI, China). Twenty milligrams of total protein were loaded on a 10% SDS polyacrylamide gel and then transferred onto a 0.45 mm PVDF membrane (300 mV, 90 min). After blocking with 5% nonfat milk at room temperature for 2 h, the membranes were incubated with anti-rabbit TH antibody (Abcam, 1:4000), anti-rabbit CaM antibody (Cell Signaling Technology, 1:1000), anti-rabbit p-CREB antibody (Cell Signaling Technology, 1:1000), anti-rabbit CREB antibody (Cell Signaling Technology, 1:1000), anti-rabbit GHS-R1a antibody (Phoenix Pharmaceuticals, 1:1000), and anti-rabbit GAPDH antibody (Cell Signaling Technology, 1:10,000) overnight at 4 °C. The membranes were then incubated with anti-rabbit secondary antibodies conjugated to horseradish peroxidase at 1:10,000 for 2 h at room temperature. Cross-reactivity was visualized using ECL Western blotting detection reagents and analyzed by scanning densitometry using an Amersham Image Quant 800 imaging system (Cytiva, USA).

Real-time polymerase chain reaction (RT-PCR)

Total RNA was isolated from the mouse SN using TRIzol reagent (Invitrogen, USA) according to the manufacturer's instructions. One microgram of RNA was transcribed into cDNA in a 20 μl reaction with a reverse-transcription kit (Vazyme, China). RT-PCR was carried out using SYBR Green Master Mix (Vazyme, China). The expression of each gene was normalized to that of GAPDH. The primer sequences were as follows: VMAT2: F = 5'-AAGAGAGGGG-TAACGCCAT-3', R = 5'-AGCAAGCACCAGGAAAGGA-3'; GAPDH: F = 5'-CAAATCCATGGCACCCTCA-3', R = 5'-ATCGCCCCACTTGATTTGG-3'.

Proximity ligation assay (PLA)

PC-12 cells were grown and fixed with 4% paraformaldehyde prepared in PBS on 6-well tissue culture slides. To visualize receptor interactions, slides or brain slices were blocked with blocking solution and incubated with mouse anti-GHS-R1a (Absin, 1:25) and rabbit anti-D₂R (Thermo Fisher Scientific, 1:50) antibodies at 4 °C overnight in a humidified chamber. The slides or

brain slices were then washed and incubated with secondary anti-rabbit/goat antibodies conjugated to PLUS and MINUS Duolink II PLA (1:5) at 37 °C for 1 h. The slides or brain slices were washed again and then incubated with ligation-ligase solution (30 min at 37 °C), followed by incubation with amplification-polymerase solution (90 min at 37 °C). PLA signals (594/624 nm) were identified as fluorescent spots under a fluorescence microscope (Leica, Germany) at room temperature and quantified with ImageJ software.

Bioluminescence resonance energy transfer (BRET)

PC-12 cells were transiently cotransfected with vectors encoding Rluc fusion (GHS-R1a-Rluc) or EGFP fusion (D₂R-EGFP) proteins. Twenty-four hours after transfection, the cells were washed twice, detached, and transferred (10⁵ cells/well) to a 96-well microplate (Corning 3600, white opaque plate) containing HEPES-buffered phenol red-free medium (Invitrogen, Life Technologies) for 24 h. The cells were then washed twice and resuspended in D-PBS (PBS containing 0.5 mM MgCl₂ and 0.1% (w/v) glucose). Coelenterazine H substrate was added to a final concentration of 5 μM. Analysis was carried out immediately at 37 °C using a Tristar LB941 plate reader (Germany).

Fluorescence resonance energy transfer (FRET)

The donor plasmid D₂R-EYFP and the receptor plasmid GHS-R1a-ECFP were cotransfected into PC-12 cells. FRET signals were detected using a Nikon A1R confocal microscope (Japan), which allowed the sequential integration of light signals detected with two filter settings. The donor channel was set to detect the excitation light of the fluorescent protein EYFP, and the acceptor channel was set to detect the emission light of the fluorescent protein ECFP. FRET from the donor channel and the acceptor channel was observed.

Microdialysis

Microdialysis guide cannulas (CMA Microdialysis AB, Sweden) were implanted into the mouse striatum. Mice were anesthetized with isoflurane gas (4% induction and 1.5%–3% maintenance; Abbott Laboratories, USA) prior to being fixed in a stereotaxic frame (RIWARD, China). The skull was adjusted so that bregma and lambda lay in the same horizontal plane to ensure that the skull was level (with ±0.1 mm tolerance), and 2 points equally distant from the midline were marked. The stereotaxic coordinates of the striatum were as follows: anterior = 0.8 mm, lateral = 1.8 mm, ventral = 3.0 mm. A hole was drilled in the skull at these coordinates, and the guide cannula was slowly lowered into the hole. The guide cannula was attached to the skull with super glue and dental cement. Following surgery, the animal was placed in a heated chamber until it awoke and moved normally.

Tubing was connected to each microsyringe. Artificial cerebrospinal fluid consisting of NaCl (147 mM), KCl (2.7 mM), CaCl₂ (1.2 mM), and MgCl₂ (0.85 mM) was used. After the mice were connected to the sampling apparatus, the room lights were turned off for the duration of the experiment. The animals were awake and freely moving while connected to the sampling apparatus to avoid any artifacts produced by anesthesia (1 μl/min). After 30 min of stabilization, cerebrospinal fluid was collected by an automated sample collector at a volume of 20 μl per mouse for 20 min, and cerebrospinal fluid DA contents were determined.

Cell viability measurement

Cell viability was measured using the Cell Counting Kit-8 (CCK-8) assay. PC-12 cells were seeded in 96-well plates, and the culture medium was replaced with 10 μl of CCK-8 solution (Solarbio, China) for 1 h at 37 °C in the dark after treatment. The absorbance at 450 nm was measured using a microplate reader (VICTOR Nivo, PerkinElmer, Finland).

Transmission electron microscopy

PC-12 cells were fixed with 2.5% glutaraldehyde for 24 h at 4 °C. Then, 1% osmic acid was added for 1 h for dehydration. The cells were embedded and incubated at 60 °C for 24 h. After sectioning, the cells were washed with ddH₂O, immersed in uranyl acetate and lead citrate solution, and then washed three times with ddH₂O. Finally, transmission electron microscopy was used for observation.

Rotarod test

A rotarod apparatus (Med Associates, USA) was used to measure balance and motor coordination. During the training period, the mice were allowed to adapt to the rotarod for 2 min without rotation. Then, the drum was slowly accelerated from a speed of 4–40 rpm for a maximum of 5 min. The latency to fall off the rotarod within this time period was recorded. Each mouse was tested twice at an interval of at least 1 h, and the results were averaged.

Open field test

The experiment was conducted in a quiet and dark environment. Exploratory activity was measured using an open-field apparatus (42 cm × 42 cm). Each mouse was placed in the center of the open-field apparatus. The center zone was defined as a square 10 cm away from each wall. The distance traveled and time spent in the zone by each animal were recorded for 10 min with a video-recording system (Smart 2.0, Panlab), as described previously.

High-performance liquid chromatography with electrochemical detection (HPLC-ECD)

After the mice were anesthetized, they were quickly decapitated, and the bilateral striata were quickly removed on ice. Eighty microliters of precooled sample pretreatment A solution (0.4 M perchloric acid) were added to accurately weigh striatal tissue. Then, the tissue was ground and centrifuged at 4 °C for 20 min at 12,000 rpm. Forty microliters of the supernatant were added to 80 μl of ice-cold pretreatment B solution (dipotassium phosphate, 300 mM; EDTA-2Na, 2 mM; citramalic acid-potassium, 20 mM), vortexed, mixed, left on ice for 1 h and centrifuged at 4 °C for 20 min at 12,000 rpm. The samples were filtered 1–2 times before being loaded into the machine. The contents of DA and its metabolites 3,4-dihydroxyphenylacetic acid (DOPAC) and homovanillic acid (HVA) in 100 μl of the supernatant were determined by HPLC-ECD (Waters, USA). The flow rate was set to 0.5–1 μl/min, and each sample was examined for 5–10 min. Each standard was tested first, and its retention time was tested as a qualitative index. A standard curve was drawn with data for standard samples (16, 8, 4, 2, 1, 0.5, 0.25, 0.125 ng/20 μl) to obtain the linear regression equation of each standard, and then the sample concentration was calculated.

Data analysis

In this experiment, GraphPad Prism 8 software was used to analyze and plot the data. One-/two-way ANOVA was used, and the experimental results are expressed as the mean ± SEM. When comparing means of more than two groups, Dunnett's test or Student's Newman-Keul test was used. *P* < 0.05 was considered statistically significant.

RESULTS

GHS-R1a and D₂R formed heterodimers both in vitro and in vivo. We assessed the coexpression of GHS-R1a and D₂R in PC-12 cells and the interactions between these two receptors. Immunofluorescence staining revealed that GHS-R1a and D₂R were colocalized in PC-12 cells (Fig. 1a). To verify the interaction between GHS-R1a and D₂R, we labeled GHS-R1a and D₂R with specific antibodies and conducted PLA (Fig. 1b), which is a sensitive method to visualize

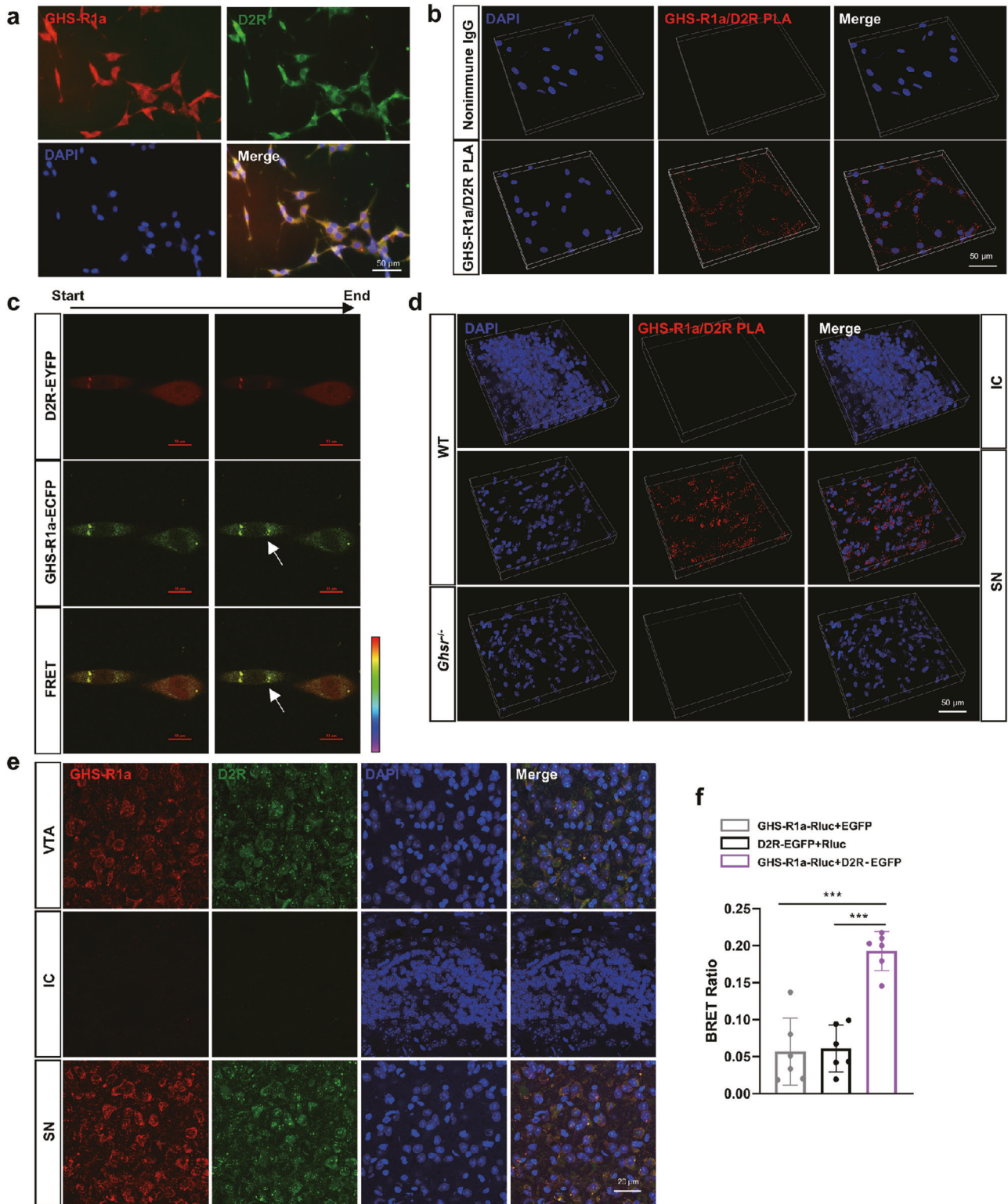


Fig. 1 GHS-R1a and D₂R formed heterodimers *in vitro* and *in vivo*. **a** Representative images for GHS-R1a and D₂R co-expressing in PC-12 cells; **b** Measurement of PLA-positive dots for GHS-R1a/D₂R heterodimers in PC-12 cells; **c** Representative confocal microscopy images for D₂R-EYFP (top, red), GHS-R1a-ECFP (middle, green) and FRET pseudo-color ratio (GHS-R1a-ECFP/D₂R-EYFP) (bottom), arrows indicate FRET imaging; **d** Measurement of PLA-positive dots for GHS-R1a/D₂R heterodimers in the SN and IC of mice; **e** Identification of neurons co-expressing GHS-R1a and D₂R in the SN, IC and VTA of mice; **f** Heterodimers of GHS-R1a and D₂R were measured by BRET. Data are depicted as bar graphs with mean ± SEM. ****P* < 0.001, *n* = 6.

and quantify protein interactions in situ [51–53]. FRET and BRET analyses were also performed to assess the interaction of GHS-R1a and D₂R in PC-12 cells. In the FRET assay, PC-12 cells were transfected with GHS-R1a-ECFP and D₂R-EYFP, and the changes in the FRET ratio were measured to assess the interaction of GHS-R1a between D₂R. In Fig. 1c, green represents sites of GHS-R1a and D₂R interaction, and the arrows indicate FRET. We were able to detect changes in the FRET ratio in PC-12 cells expressing GHS-R1a-ECFP and D₂R-EYFP. For the BRET assay, similar to the FRET assay, PC-12 cells were transfected with GHS-R1a-Rluc and D₂R-EGFP, and Western blotting showed that GHS-R1a and D₂R protein levels were significantly increased after transfection (Supplementary Fig. 1). Moreover, the BRET ratio was measured after the addition of coelenterazine. Compared with those of negative control cells transfected with GHS-R1a-Rluc + EGFP and D₂R-EGFP + Rluc, the BRET ratio of PC-12 cells cotransfected with D₂R-EGFP and GHS-R1a-Rluc were increased by 240% ($P < 0.001$) and 220% ($P < 0.001$), respectively (Fig. 1f). These results indicate that GHS-R1a and D₂R could form heterodimers in PC-12 cells.

We also assessed the colocalization of GHS-R1a and D₂R and GHS-R1a/D₂R heterodimers levels in the SN in WT mice (Fig. 1d, e). Due to the absence of D₂R expression in the WT mice [26], the islands of calleja (IC) were selected as negative controls. Since D₂R is highly expressed in the VTA [54, 55], we also tested the expression of D₂R in the VTA to verify the specificity of D₂R antibodies (Fig. 1e). Interactions between GHS-R1a and D₂R could not be observed in the IC in WT mice or the SN in *Ghsr*^{-/-} mice by PLA (Fig. 1d, e). These results suggest that GHS-R1a and D₂R were coexpressed in PC-12 cells as well as in dopaminergic neurons in the SN, where the two receptors could form heterodimers both in vitro and in vivo.

The GHS-R1a and D₂R interaction was weakened in MPP⁺/MPTP-treated cells

To evaluate the effect of 1-methyl-4-phenylpyridinium ion (MPP⁺)/MPTP on the formation of GHS-R1a/D₂R heterodimers, PC-12 cells and C57BL/6 mice were treated with MPP⁺ and MPTP, respectively. As shown in Fig. 2a, b, the number and morphology of PC-12 cells were changed, and shrinkage of the nuclear membrane and swelling of mitochondria were also observed after incubation with 2 mM MPP⁺ for 24 h. The results of morphological analysis indicated that PC-12 cells were injured by 2 mM MPP⁺. PLA showed that the number of PLA fluorescence signals was decreased by 54% in the group treated with 2 mM MPP⁺ compared with the control group (Fig. 2c, d, $P < 0.001$), indicating that the interaction between GHS-R1a and D₂R was weakened in MPP⁺-treated PC-12 cells. GHS-R1a/D₂R heterodimers were also observed in the SN in MPTP-induced PD mice model, and we detected a 36.2% reduction in the number of PLA fluorescence signals in the SN in PD mice (Fig. 2e, f, $P < 0.001$), compared with control mice, indicating that the interaction between GHS-R1a and D₂R was weakened in MPTP-induced PD mice model. These results indicate that MPP⁺/MPTP had inhibitory effects on GHS-R1a/D₂R heterodimers formation in vitro and in vivo.

Activation of GHS-R1a/D₂R heterodimers attenuated MPP⁺-induced cell injury

Then, we investigated whether activation of GHS-R1a/D₂R heterodimers could affect MPP⁺-induced cell damage. The CCK-8 assay identified 10 μM and 2 mM as the effective concentrations of QNP and MPP⁺, respectively (Fig. 3a, b). As shown in Fig. 3f, cell viability was decreased by 31.3% ($P < 0.001$) and 44.7% ($P < 0.001$) in the shRNA-NC group and shRNA-GHS-R1a group, respectively, after MPP⁺ treatment. Compared with that in the shRNA-NC group, the cell viability in the shRNA-NC-QNP group was significantly increased by 15.3% ($P = 0.002$). However, compared with that in the shRNA-NC-QNP group, the cell viability in the shRNA-GHS-R1a-QNP group was decreased by 21.1% ($P < 0.001$).

Compared with that in the shRNA-NC-QNP + MPP⁺ group, the cell viability in the shRNA-GHS-R1a-QNP + MPP⁺ group was decreased by 34.3% ($P < 0.001$). In addition, compared with that in the shRNA-NC-MPP⁺ group, the cell viability in the shRNA-NC-QNP + MPP⁺ group showed a 20.4% ($P = 0.006$) increase, which might be related to the activation of GHS-R1a/D₂R heterodimers. These results suggest that QNP could activate the GHS-R1a/D₂R heterodimers, exerting protective effects against cell death.

Activation of GHS-R1a/D₂R heterodimers improved motor function in MPTP-induced PD mice model

To determine the roles of GHS-R1a/D₂R heterodimers in PD mice, mice were subjected to behavioral tests 0.5, 1, 2, 4 and 6 h after intraperitoneal injection of 0.5/1 mg/kg QNP [53, 56–58] (Supplementary Figs. 2–4). Ultimately, 4 h and 1 mg/kg were selected as the optimal treatment duration and concentration of QNP. In the open field experiment, we measured the total distance traveled, time spent in the zone and average speed of the mice. Our results showed that compared with the WT-NS and *Ghsr*^{-/-}-NS groups, the WT-MPTP and *Ghsr*^{-/-}-MPTP groups exhibited a 33.9% ($P < 0.001$) and 25.9% ($P = 0.003$) reduction in total distance traveled, respectively (Fig. 4c). Compared with that of the WT-NS and *Ghsr*^{-/-}-NS groups, the mean speed of the WT-MPTP and *Ghsr*^{-/-}-MPTP groups was decreased by 26.6% ($P = 0.037$) and 16.1%, respectively (Fig. 4e). The total distance traveled was decreased by 17.0% ($P = 0.039$) in the *Ghsr*^{-/-}-QNP group compared with the WT-QNP group (Fig. 4c). The total distance traveled, the mean speed and the time spent in the zone were increased by 34.8% ($P = 0.029$), 28.8% ($P = 0.008$), and decreased by 41.4% ($P = 0.023$), respectively, in the WT-QNP + MPTP group compared with the WT-MPTP group. Compared with the WT-QNP + MPTP group, the *Ghsr*^{-/-}-QNP + MPTP group exhibited a 20.5% ($P = 0.011$) reduction in total distance traveled, a 112.1% ($P < 0.001$) increase in the time spent in the zone, and a 31.4% ($P = 0.003$) decrease in mean speed (Fig. 4b–e).

Moreover, in the rotarod test, compared with the WT-NS and *Ghsr*^{-/-}-NS groups, the WT-MPTP and *Ghsr*^{-/-}-MPTP groups exhibited a 64.9% ($P = 0.009$) and 79.7% ($P = 0.001$) reduction in time spent on the rod, respectively (Fig. 4f). The time spent on the rod was increased by 151.9% ($P = 0.043$) in the WT-QNP + MPTP group compared with the WT-MPTP group. The time spent on the rod was decreased by 68.2% ($P = 0.022$) in the *Ghsr*^{-/-}-QNP group compared with the WT-QNP group. The time spent on the rod was decreased by 73.1% ($P = 0.004$) in the *Ghsr*^{-/-}-QNP + MPTP group compared with the WT-QNP + MPTP group (Fig. 4f). The above results suggest that activation of the GHS-R1a/D₂R heterodimers by QNP could improve the motor function in MPTP-induced PD mice model.

Then, extracellular DA contents in the different groups were determined by microdialysis. Our results showed that extracellular DA contents were increased by 105.1% ($P = 0.002$) in the WT-QNP group compared with the WT-NS group. And the extracellular DA contents were 54.3% ($P < 0.001$) lower in the *Ghsr*^{-/-}-QNP group than in the WT-QNP group and 155.1% ($P = 0.041$) higher in the WT-QNP + MPTP group than in the WT-MPTP group (Fig. 4g). The above results indicate that the improvement in the motor function of MPTP-treated PD mice model might have been associated with increased extracellular DA contents in the striatum.

The CaM/CREB signaling pathway mediated the neuroprotective effect of the GHS-R1a/D₂R heterodimers in PD

To verify the mechanism underlying the increase in extracellular DA contents in the striatum induced by QNP, we assessed the expression of CaM/CREB pathway-related proteins and their downstream target proteins, TH and VMAT2. Our results showed that CaM protein levels in the SN were increased by 149% ($P = 0.008$) in the WT-QNP + MPTP group compared with the WT-MPTP group. CaM protein levels in the SN were decreased by

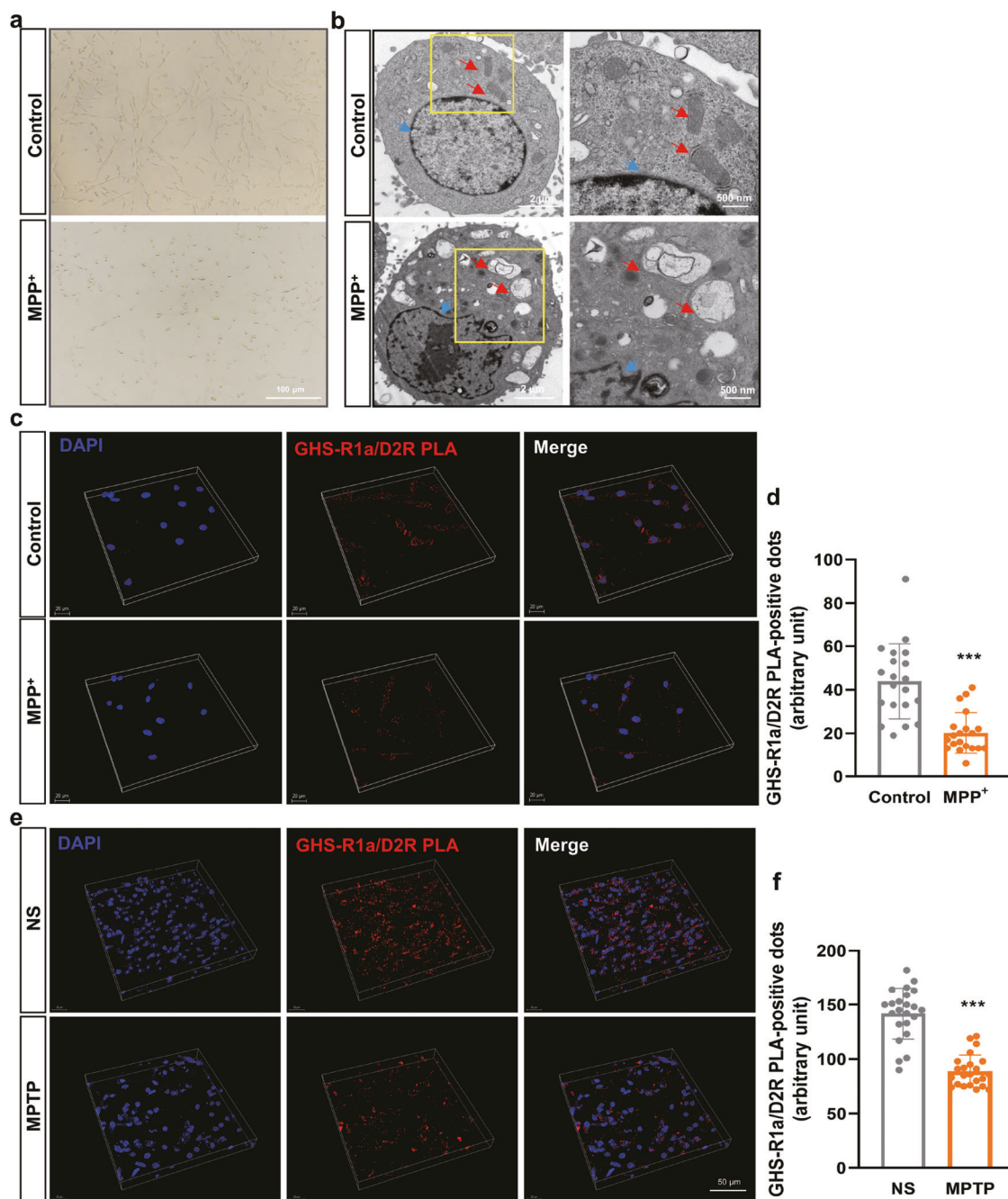


Fig. 2 Effect of MPP⁺ and MPTP on the interaction of GHS-R1a and D2R *in vitro* and *in vivo*. **a** The decrease of PC-12 cell density induced by MPP⁺ was observed by inverted fluorescence microscope; **b** The ultrastructure of PC-12 cells treated with MPP⁺ was observed by transmission electron microscope. Red arrows indicate mitochondria and blue arrows indicate the nuclear membrane; **c** Representative images of GHS-R1a/D₂R PLA-positive dots in PC-12 cells of control and MPP⁺ group; **d** Analysis of GHS-R1a/D₂R PLA-positive dots in the PC-12 cells treated with vehicle or 2 mM MPP⁺ for 24 h; **e** Representative images of GHS-R1a/D₂R PLA-positive dots in WT mice and PD mice; **f** Analysis of GHS-R1a/D₂R PLA-positive dots in the MPTP-treated PD mice. Data are depicted as bar graphs with as mean ± SEM. ****P* < 0.001, *n* = 20.

74.8% (*P* < 0.001) in the *Ghsr*^{-/-}-QNP + MPTP group compared with the WT-QNP + MPTP group (Fig. 5a, b).

Then, we measured the protein levels of p-CREB and CREB. The p-CREB/CREB ratio in the SN was increased by 101.3% (*P* = 0.009) in the WT-QNP group compared with the WT-NS group. The p-CREB/CREB ratio in the SN was decreased by 55.4% (*P* = 0.007) in the *Ghsr*^{-/-}-QNP group compared with the WT-QNP group. Moreover, the p-CREB/CREB ratio in the SN was increased by 177.4% (*P* = 0.002) in the WT-QNP + MPTP group compared with

the WT-MPTP group. The p-CREB/CREB ratio in the SN was decreased by 50.3% (*P* = 0.024) in the *Ghsr*^{-/-}-QNP + MPTP group compared with the WT-QNP + MPTP group (Fig. 5a, c). These results demonstrate that activation of the GHS-R1a/D₂R heterodimers could increase CaM protein levels and the p-CREB/CREB ratio in the SN in MPTP-induced PD mice model.

Subsequently, we evaluated the expression of TH by Western blotting. The results showed that TH protein levels in the SN were increased by 79.8% (*P* < 0.001) in the WT-QNP group

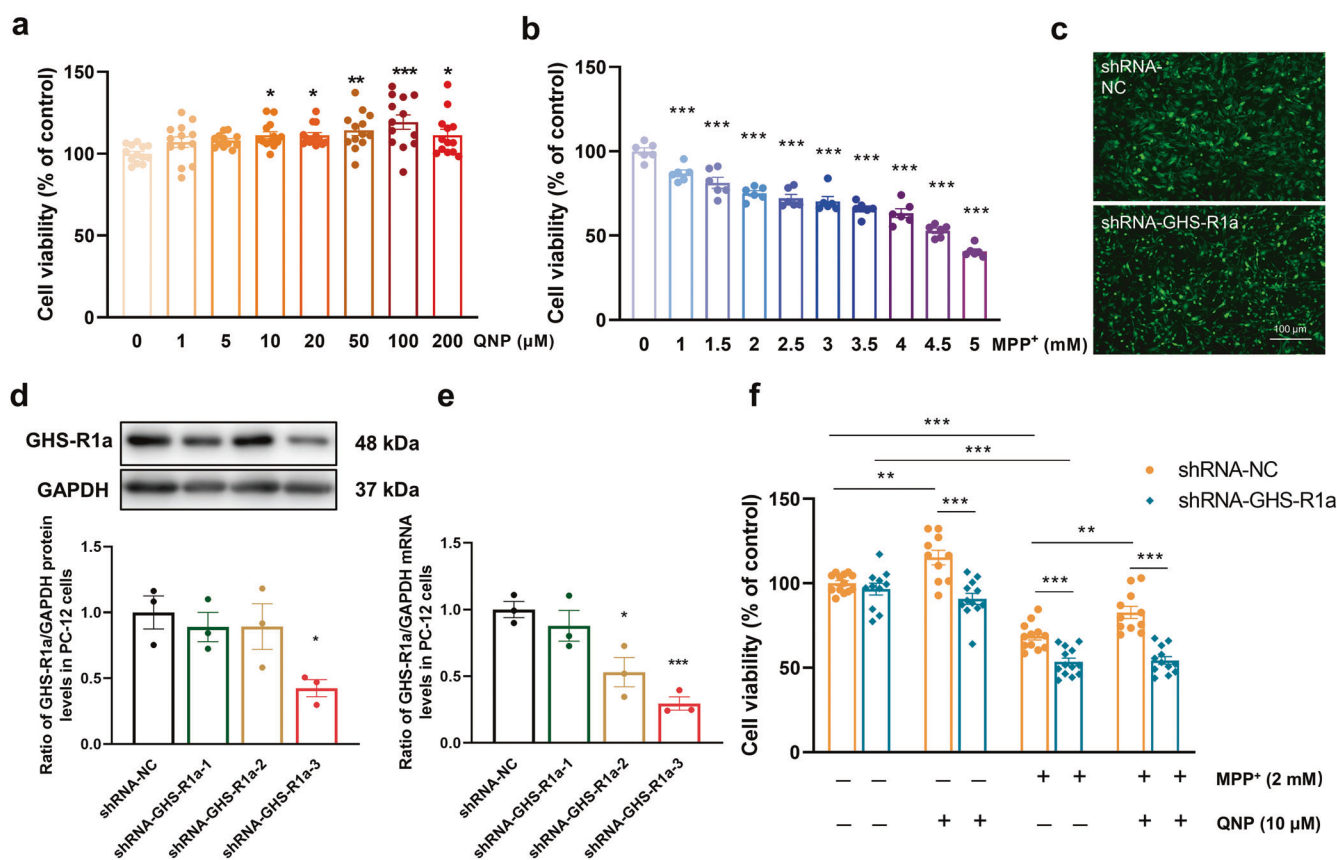


Fig. 3 Effect of GHS-R1a/D₂R heterodimers activation on cell viability. Effects of QNP (a) and MPP⁺ (b) on cell viability at indicated concentrations in PC-12 cells; c The efficiency of virus infection was detected by fluorescence microscope; d, e The protein and mRNA levels of GHS-R1a were decreased in shRNA-GHS-R1a-3 cells; f Pre-incubation with QNP (10 μM) antagonized MPP⁺ (2 mM)-induced reduction in cell viability in shRNA-NC group, as determined by CCK-8 assay. Data are depicted as bar graphs with mean ± SEM. **P* < 0.05 vs. control, ***P* < 0.01 vs. control, ****P* < 0.001 vs. control, **P* < 0.05 vs. shRNA-NC, ****P* < 0.001 vs. shRNA-NC, *n* = 12, 12, 3, 3, 12.

compared with the WT-NS group. Compared with the WT-QNP group, the *Ghsr*^{-/-}-QNP group exhibited a 62.6% (*P* < 0.001) decrease in TH protein levels in the SN. Similarly, TH protein expression in the SN was 69.1% (*P* = 0.035) higher in the WT-QNP + MPTP group than in the WT-MPTP group. TH protein levels in the SN were decreased by 47% (*P* = 0.012) in the *Ghsr*^{-/-}-QNP + MPTP group compared with the WT-QNP + MPTP group (Fig. 5a, d). These results suggest that activation of the GHS-R1a/D₂R heterodimers promoted TH protein expression in the SN in MPTP-induced PD mice model.

Finally, the changes in VMAT2 mRNA levels were measured by RT-PCR, and the results are shown in Fig. 5e. VMAT2 mRNA expression in the SN was increased by 48.8% (*P* = 0.025) in the WT-QNP group compared with the WT-NS group, while compared with that in the WT-QNP group, VMAT2 mRNA expression in the *Ghsr*^{-/-}-QNP group was decreased by 48.2% (*P* < 0.001). These results indicate that the activation of GHS-R1a/D₂R heterodimers could promote the transcription of the CREB downstream target VMAT2 but did not affect the mRNA expression of VMAT2 in the SN of MPTP-induced PD mice model.

DISCUSSION

In the present study, we demonstrated that endogenous GHS-R1a and D₂R could form heterodimers both in vitro and in vivo and that GHS-R1a/D₂R heterodimers formation was reduced in MPTP-induced PD mice model. Activation of GHS-R1a/D₂R heterodimers by QNP conferred neuroprotection in PD mice by promoting DA synthesis and release. The underlying mechanisms might be

related to the elevation of CaM and p-CREB protein levels, resulting in enhanced TH expression (Fig. 6).

Several recent studies have shown that GHS-R1a is able to form heterodimers with two types of dopamine receptors, D₁R and D₂R [23, 59–61]. In the brain, D₁R is highly expressed in the striatum, nucleus accumbens, olfactory bulb, amygdala and frontal cortex, while D₂R is mainly expressed in the SN, striatum, nucleus accumbens, olfactory tubercle, VTA, hypothalamus and hippocampus [62, 63]. D₂R, but not D₁R, is expressed in the presynaptic membranes of dopaminergic neurons in the SN [64–69], where GHS-R1a is also expressed [60, 70, 71]. This provides a basis for the formation of the GHS-R1a/D₂R heterodimers in dopaminergic neurons in the SN. In our study, for the first time, we observed that GHS-R1a and D₂R could form heterodimers in PC-12 cells and dopaminergic neurons.

To verify the function of GHS-R1a/D₂R heterodimers in PD, QNP was used to induce the activation of GHS-R1a/D₂R heterodimers [59, 60, 72]. In vitro, we observed that QNP alone enhanced cell viability in the shRNA-NC group and MPP⁺-treated shRNA-NC group but not in the shRNA-GHS-R1a group. Furthermore, some studies have also shown that the length of primary dendrites, number of dendrites and cell body area of midbrain dopaminergic neurons derived from human-induced pluripotent stem cells were significantly increased after QNP treatment, and these phenomena may be related to the PI3K-ERK1/2 signaling pathway [73]. In vivo, we observed that QNP could increase the total distance traveled and mean speed in the open field test and time spent on the rod in the rotarod test or even reverse the decreases in these parameters caused by MPTP

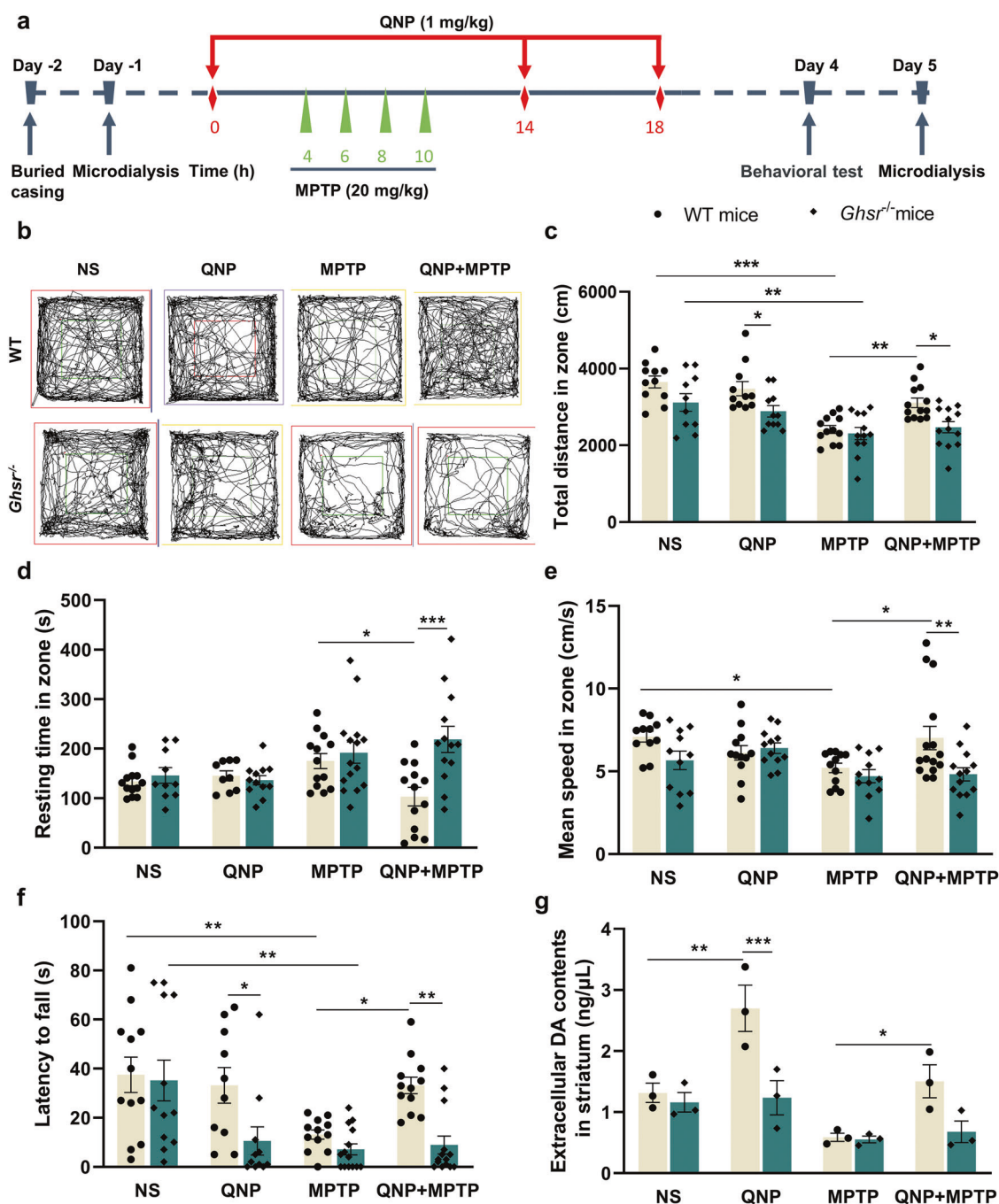


Fig. 4 Effects of GHS-R1a/D₂R heterodimers activation on motor abilities in MPTP-induced PD mice model. **a** Schematic diagram of animal modeling; **b** The trajectory of open field in different groups; **c–e** The distance traveled, resting time and mean speed in the open field were evaluated; **f** The residence time of mice in different groups on rotarod was assessed by the rotarod test; **g** Extracellular DA contents in the striatum were determined by microdialysis. Data are depicted as bar graphs with mean ± SEM, **P* < 0.05, ***P* < 0.01, ****P* < 0.001, *n* = 10–13, 3.

in WT mice. Moreover, we found that the extracellular DA contents in MPTP-treated WT mice were increased by QNP treatment; however, none of these changes were observed in GHS-R1a knockout mice. These results indicated that activation of GHS-R1a/D₂R heterodimers by QNP could increase extracellular DA contents in the striatum, ultimately improving motor performance in MPTP-induced PD mice model. Similarly, Shao et al. found that repeated QNP treatment significantly reduced SN inflammation and resisted MPTP-induced dopaminergic neuron damage [74], but the mechanisms underlying the effects of QNP have not been elucidated.

In the nigral dopaminergic neurons of PD patients, neuroplasticity and axonal and synaptic plasticity can be regulated by the CREB signaling pathway [36]. Inhibition of CREB activation in vitro leads to neuronal differentiation impairment. The survival rate of newborn neurons in transgenic mice with CREB deficiency is low [34]. This evidence suggests that the CREB pathway is of great importance in maintaining normal nervous system function. In our study, we observed that the expression of CaM and the p-CREB/CREB ratio in the SN were decreased in MPTP-induced PD mice model. Activation of GHS-R1a/D₂R heterodimers by QNP could promote CaM-mediated CREB phosphorylation. CREB is involved

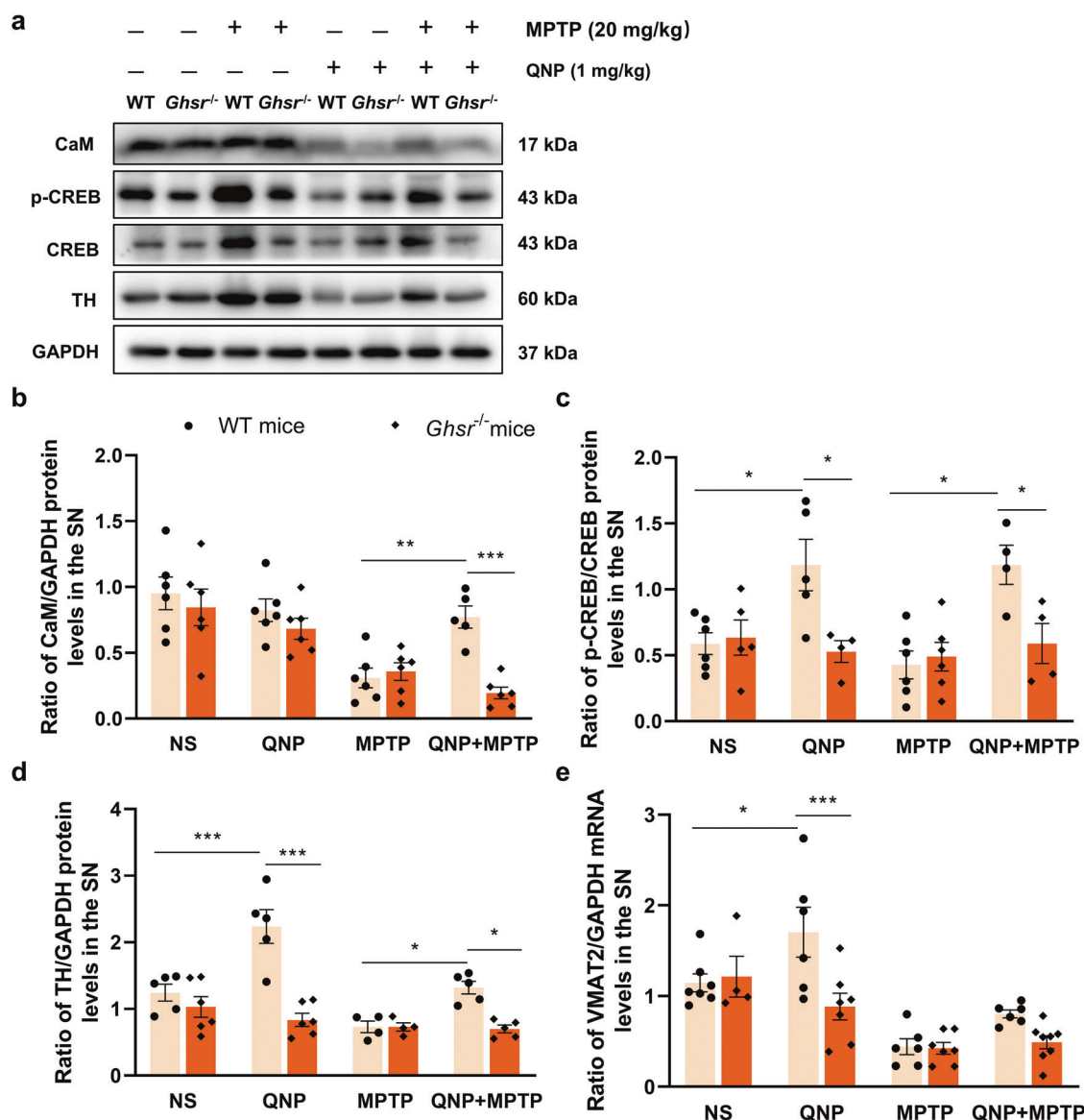


Fig. 5 CaM/CREB pathway involved in the protection of dopaminergic neurons by GHS-R1a/D₂R heterodimers activation. **a–d** Western blotting was applied to detect the levels of CaM, p-CREB, CREB and TH in the SN of WT and *Ghsr*^{-/-} mice treated with QNP and MPTP; **e** VMAT2 mRNA levels in the SN of WT and *Ghsr*^{-/-} mice treated with QNP and MPTP. Data are depicted as bar graphs with mean ± SEM, **P* < 0.05, ***P* < 0.01, ****P* < 0.001, *n* = 5.

in the formation of DNA/protein complexes between the cAMP response element and the TH and VMAT2 genes and, together with CREB-binding protein, regulates the transcription of genes [46, 75]. Then, we investigated the effect of GHS-R1a/D₂R heterodimers activation on VMAT2 and TH expression in MPTP-induced PD mice model.

VMAT2, one of the downstream targets of CREB, is responsible for mediating the release of DA from the presynaptic membrane [76–79]. In our study, we did not observe any significant changes in VMAT2 mRNA levels after QNP treatment. TH is the rate-limiting enzyme of DA synthesis by dopaminergic neurons [80] and plays an important role in DA biosynthesis. TH can be used as a marker of dopaminergic neurons, and the pathogenesis of PD is related to a reduction in TH levels [81]. Previous studies have shown that the mRNA and protein levels of TH in the SN and TH enzyme activity were decreased in PD animal models [82–85]. Relevant clinical experiments have also indicated that TH gene and protein levels and activity in the SN exhibit abnormal changes in PD patients [86], leading to the clinical

symptoms of the disease. Injection of TH-transfected nerve cells into the striata of PD rats can relieve PD-related symptoms [87]. Moreover, delivery of human-derived TH into the striata of PD rats can ameliorate PD symptoms, enhance TH activity, increase DA synthesis and alleviate abnormal rotation behavior [88, 89]. We observed that TH protein expression was significantly upregulated in WT mice and MPTP-induced PD mice model after QNP treatment. These results indicated that GHS-R1a/D₂R heterodimers activation could promote TH expression but not VMAT2 expression through the CaM/CREB pathway. TH could promote DA synthesis, increase extracellular DA contents in the striatum, and ultimately promote motor function improvement in animals. However, this selective regulation of VMAT2 and TH expression may be related to the preferential nature of the regulatory effect of CREB after activation by GHS-R1a/D₂R heterodimers [90–92], and whether other regulatory mechanisms exist remains to be elucidated.

In conclusion, GHS-R1a and D₂R were expressed and could form heterodimers in dopaminergic cells and neurons in the SN.

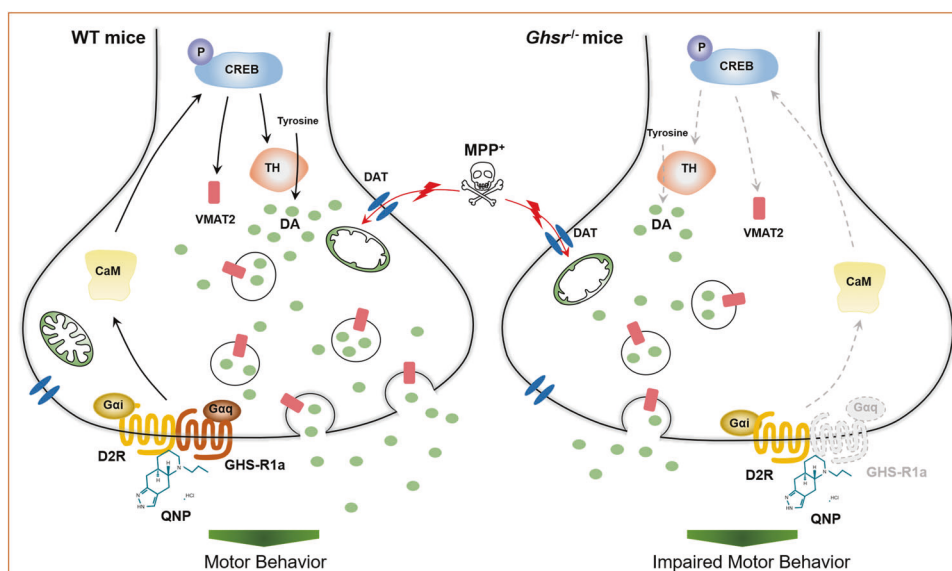


Fig. 6 The role of GHS-R1a/D₂R heterodimers activation in dopaminergic neurons. GHS-R1a and D₂R receptors form heterodimers in dopaminergic neurons, GHS-R1a/D₂R heterodimers activation upregulates TH expression through CaM-mediated CREB signaling pathway, promotes synthesis and release of DA, and antagonizes MPTP-induced behavioral changes in WT mice.

Activation of GHS-R1a/D₂R heterodimers by QNP significantly improved the motor function of MPTP-induced PD mice, and the mechanism might be related to GHS-R1a/D₂R heterodimers activation, which regulates the CaM/CREB pathway, promotes the synthesis and release of DA by upregulating TH expression, and ultimately alleviates MPTP-induced injury in mice. Considering that GHS-R1a is highly expressed in the SN, has high constitutive activity, and dimerizes with other receptors, the present study might provide new targets for the pharmacological treatment of PD.

DATA AVAILABILITY

All data generated or analyzed during this study are included in this published article and its Supplementary files.

ACKNOWLEDGEMENTS

National Natural Science Foundation of China, Grant/Award Numbers: 32171131, 82071429 and 32270113; Natural Science Foundation of Shandong Province, Grant/Award Numbers: 2021ZDSYS11, ZR2019ZD31, ZR2022MC098, ZR2020MC072 and ZR2020QH125; Taishan Scholars Construction Project.

AUTHOR CONTRIBUTIONS

HJ and XXD conceived and designed research. TTT, MND, XYZ, LC and XX performed experiments and analyzed data. TTT wrote the manuscript. HJ, XD, MXB, QJ, XC and CLY revised the manuscript.

ADDITIONAL INFORMATION

Supplementary information The online version contains supplementary material available at <https://doi.org/10.1038/s41401-023-01063-0>.

Competing interests: The authors declare no competing interests.

Ethical approval: All protocols were approved by the Animal Ethics Committee of Qingdao University.

REFERENCES

1. Tolosa E, Garrido A, Scholz SW, Poewe W. Challenges in the diagnosis of Parkinson's disease. *Lancet Neurol.* 2021;20:385–97.

- Bloem BR, Okun MS, Klein C. Parkinson's disease. *Lancet.* 2021;397:2284–303.
- Mahoney-Sánchez L, Bouchaoui H, Ayton S, Devos D, Duce JA, Devedjian JC. Ferroptosis and its potential role in the pathophysiology of Parkinson's Disease. *Prog Neurobiol.* 2021;196:101890.
- Bi MX, Du XX, Xiao X, Dai YY, Jiao Q, Chen X, et al. Deficient immunoproteasome assembly drives gain of α -synuclein pathology in Parkinson's disease. *Redox Biol.* 2021;47:102167.
- Howard AD, Feighner SD, Cully DF, Arena JP, Liberatore PA, Rosenblum CI, et al. A receptor in pituitary and hypothalamus that functions in growth hormone release. *Science.* 1996;273:974–7.
- Li HZ, Shou LL, Shao XX, Li N, Liu YL, Xu ZG, et al. LEAP2 has antagonized the ghrelin receptor GHSR1a since its emergence in ancient fish. *Amino Acids.* 2021;53:939–49.
- Shi LM, Bian XL, Qu ZQ, Ma ZG, Zhou Y, Wang KW, et al. Peptide hormone ghrelin enhances neuronal excitability by inhibition of Kv7/KCNQ channels. *Nat Commun.* 2013;4:1435.
- Suda Y, Kuzumaki N, Sone T, Narita M, Tanaka K, Hamada Y, et al. Down-regulation of ghrelin receptors on dopaminergic neurons in the substantia nigra contributes to Parkinson's disease-like motor dysfunction. *Mol Brain.* 2018;11:6.
- Huang HJ, Chen XR, Han QQ, Wang J, Pilot A, Yu R, et al. The protective effects of Ghrelin/GHSR on hippocampal neurogenesis in CUMS mice. *Neuropharmacology.* 2019;155:31–43.
- Gross JD, Kim DW, Zhou Y, Jansen D, Slosky LM, Clark NB, et al. Discovery of a functionally selective ghrelin receptor (GHSR(1a)) ligand for modulating brain dopamine. *Proc Natl Acad Sci USA.* 2022;119:e2112397119.
- Mear Y, Enjalbert A, Thirion S. GHS-R1a constitutive activity and its physiological relevance. *Front Neurosci.* 2013;7:87.
- Holst B, Holliday ND, Bach A, Elling CE, Cox HM, Schwartz TW. Common structural basis for constitutive activity of the ghrelin receptor family. *J Biol Chem.* 2004;279:53806–17.
- Damian M, Marie J, Leyris JP, Fehrentz JA, Verdié P, Martinez J, et al. High constitutive activity is an intrinsic feature of ghrelin receptor protein: a study with a functional monomeric GHS-R1a receptor reconstituted in lipid discs. *J Biol Chem.* 2012;287:3630–41.
- Rouault AAJ, Rosselli-Murai LK, Hernandez CC, Gimenez LE, Tall GG, Sebag JA. The GPCR accessory protein MRAP2 regulates both biased signaling and constitutive activity of the ghrelin receptor GHSR1a. *Sci Signal.* 2020;13:eaa4569.
- Xiao X, Bi MX, Jiao Q, Chen X, Du XX, Jiang H. A new understanding of GHSR1a-independent of ghrelin activation. *Ageing Res Rev.* 2020;64:101187.
- Rediger A, Tarnow P, Bickenbach A, Schaefer M, Krude H, Gruters A, et al. Heterodimerization of hypothalamic G-protein-coupled receptors involved in weight regulation. *Obes Facts.* 2009;2:80–6.
- Girardet C, Mavrikaki M, Southern MR, Smith RG, Butler AA. Assessing interactions between *Ghsr* and *Mc3r* reveals a role for *AgRP* in the expression of food anticipatory activity in male mice. *Endocrinology.* 2014;155:4843–55.

18. Schellekens H, van Oeffelen WE, Dinan TG, Cryan JF. Promiscuous dimerization of the growth hormone secretagogue receptor (GHS-R1a) attenuates ghrelin-mediated signaling. *J Biol Chem*. 2013;288:181–91.
19. Schellekens H, De Francesco PN, Kandil D, Theeuwes WF, McCarthy T, van Oeffelen WE, et al. Ghrelin's orexigenic effect is modulated via a serotonin 2C receptor interaction. *ACS Chem Neurosci*. 2015;6:1186–97.
20. Xue QJ, Bai B, Ji BY, Chen XY, Wang CM, Wang PX, et al. Ghrelin through GHSR1a and OX1R heterodimers reveals a galphas-cAMP-cAMP response element binding protein signaling pathway in vitro. *Front Mol Neurosci*. 2018;11:245.
21. Suarez AN, Liu CM, Cortella AM, Noble EE, Kanoski SE. Ghrelin and orexin interact to increase meal size through a descending hippocampus to hindbrain signaling pathway. *Biol Psychiatry*. 2020;87:1001–11.
22. Müller TD, Müller A, Yi CX, Habegger KM, Meyer CW, Gaylann BD, et al. The orphan receptor Gpr83 regulates systemic energy metabolism via ghrelin-dependent and ghrelin-independent mechanisms. *Nat Commun*. 2013;4:1968.
23. Kern A, Mavrikaki M, Ullrich C, Albarran-Zeckler R, Brantley AF, Smith RG. Hippocampal dopamine/DRD1 signaling dependent on the ghrelin receptor. *Cell*. 2015;163:1176–90.
24. Bunzow JR, Van Tol HH, Grandy DK, Albert P, Salon J, Christie M, et al. Cloning and expression of a rat D2 dopamine receptor cDNA. *Nature*. 1988;336:783–7.
25. Xiao P, Yan W, Gou L, Zhong YN, Kong L, Wu C, et al. Ligand recognition and allosteric regulation of DRD1-Gs signaling complexes. *Cell*. 2021;184:943–56.e18.
26. Monti JM, Monti D. The involvement of dopamine in the modulation of sleep and waking. *Sleep Med Rev*. 2007;11:113–33.
27. Bello EP, Casas-Cordero R, Galinanes GL, Casey E, Belluscio MA, Rodriguez V, et al. Inducible ablation of dopamine D2 receptors in adult mice impairs locomotion, motor skill learning and leads to severe parkinsonism. *Mol Psychiatry*. 2017;22:595–604.
28. Kobayashi M, Iaccarino C, Saiardi A, Heidt V, Bozzi Y, Picetti R, et al. Simultaneous absence of dopamine D1 and D2 receptor-mediated signaling is lethal in mice. *Proc Natl Acad Sci USA*. 2004;101:11465–70.
29. Carlezon WA Jr., Duman RS, Nestler EJ. The many faces of CREB. *Trends Neurosci*. 2005;28:436–45.
30. Kim KS, Lee MK, Carroll J, Joh TH. Both the basal and inducible transcription of the tyrosine hydroxylase gene are dependent upon a cAMP response element. *J Biol Chem*. 1993;268:15689–95.
31. Sakamoto KM, Frank DA. CREB in the pathophysiology of cancer: implications for targeting transcription factors for cancer therapy. *Clin Cancer Res*. 2009;15:2583–7.
32. Wang H, Xu J, Lazarovici P, Quirion R, Zheng W. cAMP response element-binding protein (CREB): a possible signaling molecule link in the pathophysiology of schizophrenia. *Front Mol Neurosci*. 2018;11:255.
33. Lane-Ladd SB, Pineda J, Boundy VA, Pfeuffer T, Krupinski J, Aghajanian GK, et al. CREB (cAMP response element-binding protein) in the locus coeruleus: biochemical, physiological, and behavioral evidence for a role in opiate dependence. *J Neurosci*. 1997;17:7890–901.
34. Giachino C, De Marchis S, Giampietro C, Parlato R, Perroteau I, Schütz G, et al. cAMP response element-binding protein regulates differentiation and survival of newborn neurons in the olfactory bulb. *J Neurosci*. 2005;25:10105–18.
35. Ao H, Ko SW, Zhuo M. CREB activity maintains the survival of cingulate cortical pyramidal neurons in the adult mouse brain. *Mol Pain*. 2006;2:15.
36. Elstner M, Morris CM, Heim K, Bender A, Mehta D, Jaros E, et al. Expression analysis of dopaminergic neurons in Parkinson's disease and aging links transcriptional dysregulation of energy metabolism to cell death. *Acta Neuropathol*. 2011;122:75–86.
37. Wei F, Qiu CS, Liaw J, Robinson DA, Ho N, Chatila T, et al. Calcium calmodulin-dependent protein kinase IV is required for fear memory. *Nat Neurosci*. 2002;5:573–9.
38. Brami-Cherrier K, Valjent E, Garcia M, Pages C, Hipskind RA, Caboche J. Dopamine induces a PI3-kinase-independent activation of Akt in striatal neurons: a new route to cAMP response element-binding protein phosphorylation. *J Neurosci*. 2002;22:8911–21.
39. Lonze BE, Ginty DD. Function and regulation of CREB family transcription factors in the nervous system. *Neuron*. 2002;35:605–23.
40. Yan XD, Liu JF, Ye ZX, Huang JH, He F, Xiao W, et al. CaMKII-mediated CREB phosphorylation is involved in Ca²⁺-induced BDNF mRNA transcription and neurite outgrowth promoted by electrical stimulation. *PLoS One*. 2016;11:e0162784.
41. Song XF, Cui ZQ, He JH, Yang T, Sun XH. κ -opioid receptor agonist, U50488H, inhibits pyroptosis through NLRP3 via the Ca(2+)/CaMKII/CREB signaling pathway and improves synaptic plasticity in APP/PS1 mice. *Mol Med Rep*. 2021;24:529.
42. Kawahata I, Fukunaga K. Degradation of tyrosine hydroxylase by the ubiquitin-proteasome system in the pathogenesis of Parkinson's disease and dopa-responsive dystonia. *Int J Mol Sci*. 2020;21:3779.
43. Nagatsu T, Nakashima A, Watanabe H, Ito S, Wakamatsu K. Neuromelanin in Parkinson's disease: tyrosine hydroxylase and tyrosinase. *Int J Mol Sci*. 2022;23:4176.
44. Tunbridge EM, Narajos M, Harrison CH, Beresford C, Cipriani A, Harrison PJ. Which dopamine polymorphisms are functional? Systematic review and meta-analysis of COMT, DAT, DBH, DDC, DRD1-5, MAOA, MAOB, TH, VMAT1, and VMAT2. *Biol Psychiatry*. 2019;86:608–20.
45. Mulvihill KG. Presynaptic regulation of dopamine release: role of the DAT and VMAT2 transporters. *Neurochem Int*. 2019;122:94–105.
46. Lewis-Tuffin LJ, Quinn PG, Chikaraishi DM. Tyrosine hydroxylase transcription depends primarily on cAMP response element activity, regardless of the type of inducing stimulus. *Mol Cell Neurosci*. 2004;25:536–47.
47. Tinti C, Yang C, Seo H, Conti B, Kim C, Joh TH, et al. Structure/function relationship of the cAMP response element in tyrosine hydroxylase gene transcription. *J Biol Chem*. 1997;272:19158–64.
48. Lim J, Yang C, Hong SJ, Kim KS. Regulation of tyrosine hydroxylase gene transcription by the cAMP-signaling pathway: involvement of multiple transcription factors. *Mol Cell Biochem*. 2000;212:51–60.
49. Wiemerslage L, Schultz BJ, Ganguly A, Lee D. Selective degeneration of dopaminergic neurons by MPP⁺ and its rescue by D2 autoreceptors in *Drosophila* primary culture. *J Neurochem*. 2013;126:529–40.
50. Moriguchi S, Yabuki Y, Fukunaga K. Reduced calcium/calmodulin-dependent protein kinase II activity in the hippocampus is associated with impaired cognitive function in MPTP-treated mice. *J Neurochem*. 2012;120:541–51.
51. Weibrecht I, Leuchowius KJ, Clausson CM, Conze T, Jarvis M, Howell WM, et al. Proximity ligation assays: a recent addition to the proteomics toolbox. *Expert Rev Proteom*. 2010;7:401–9.
52. Tian J, Guo L, Sui SM, Driskill C, Phensy A, Wang Q, et al. Disrupted hippocampal growth hormone secretagogue receptor 1 α interaction with dopamine receptor D1 plays a role in Alzheimer's disease. *Sci Transl Med*. 2019;11:eaav6278.
53. Poulard C, Jacquemetton J, Pham TH, Le Romancer M. Using proximity ligation assay to detect protein arginine methylation. *Methods*. 2020;175:66–71.
54. Krabbe S, Duda J, Schiemann J, Poetschke C, Schneider G, Kandel ER, et al. Increased dopamine D2 receptor activity in the striatum alters the firing pattern of dopamine neurons in the ventral tegmental area. *Proc Natl Acad Sci USA*. 2015;112:E1498–506.
55. Peng BB, Xu QK, Liu J, Guo S, Borgland SL, Liu S. Corticosterone attenuates reward-seeking behavior and increases anxiety via D2 receptor signaling in ventral tegmental area dopamine neurons. *J Neurosci*. 2021;41:1566–81.
56. Koulchitsky S, Delaïresse C, Beeken T, Monteforte A, Dethier J, Quertemont E, et al. Activation of D2 autoreceptors alters cocaine-induced locomotion and slows down local field oscillations in the rat ventral tegmental area. *Neuropharmacology*. 2016;108:120–7.
57. Horvitz JC, Williams G, Joy R. Time-dependent actions of D2 family agonist quinpirole on spontaneous behavior in the rat: dissociation between sniffing and locomotion. *Sychopharmacology*. 2001;154:350–5.
58. Escobar AP, González MP, Meza RC, Noches V, Henny P, Gysling K, et al. Mechanisms of kappa opioid receptor potentiation of dopamine D2 receptor function in quinpirole-induced locomotor sensitization in rats. *Int J Neuropsychopharmacol*. 2017;20:660–9.
59. Kern A, Albarran-Zeckler R, Walsh HE, Smith RG. Apo-ghrelin receptor forms heteromers with DRD2 in hypothalamic neurons and is essential for anorexigenic effects of DRD2 agonism. *Neuron*. 2012;73:317–32.
60. Cordisco Gonzalez S, Mustafá ER, Rodriguez SS, Perello M, Raingo J. Dopamine receptor type 2 and ghrelin receptor coexpression alters Ca(V)2.2 modulation by G protein signaling cascades. *ACS Chem Neurosci*. 2020;11:3–13.
61. Jiang H, Betancourt L, Smith RG. Ghrelin amplifies dopamine signaling by cross talk involving formation of growth hormone secretagogue receptor/dopamine receptor subtype 1 heterodimers. *Mol Endocrinol*. 2006;20:1772–85.
62. Smiley JF, Levey AI, Ciliax BJ, Goldman-Rakic PS. D1 dopamine receptor immunoreactivity in human and monkey cerebral cortex: predominant and extrasynaptic localization in dendritic spines. *Proc Natl Acad Sci USA*. 1994;91:5720–4.
63. Beaulieu JM, Gainetdinov RR. The physiology, signaling, and pharmacology of dopamine receptors. *Pharmacol Rev*. 2011;63:182–217.
64. Hurd YL, Suzuki M, Sedvall GC. D1 and D2 dopamine receptor mRNA expression in whole hemisphere sections of the human brain. *J Chem Neuroanat*. 2001;22:127–37.
65. Björklund A, Dunnett SB. Dopamine neuron systems in the brain: an update. *Trends Neurosci*. 2007;30:194–202.
66. Harrison MB, Wiley RG, Wooten GF. Selective localization of striatal D1 receptors to striatonigral neurons. *Brain Res*. 1990;528:317–22.
67. Yung KK, Bolam JP, Smith AD, Hersch SM, Ciliax BJ, Levey AI. Immunocytochemical localization of D1 and D2 dopamine receptors in the basal ganglia of the rat: light and electron microscopy. *Neuroscience*. 1995;65:709–30.
68. Calabresi P, Picconi B, Tozzi A, Ghiglieri V, Di Filippo M. Direct and indirect pathways of basal ganglia: a critical reappraisal. *Nat Neurosci*. 2014;17:1022–30.
69. Calipari ES, Sun H, Eldeeb K, Luessen DJ, Feng X, Howlett AC, et al. Amphetamine self-administration attenuates dopamine D2 autoreceptor function. *Neuropsychopharmacology*. 2014;39:1833–42.

70. Weiss N, Zamponi GW. All roads lead to presynaptic calcium channel inhibition by the ghrelin receptor: separate agonist-dependent and -independent signaling pathways. *J Gen Physiol.* 2015;146:201–4.
71. Martínez Damonte V, Rodríguez SS, Raingo J. Growth hormone secretagogue receptor constitutive activity impairs voltage-gated calcium channel-dependent inhibitory neurotransmission in hippocampal neurons. *J Physiol.* 2018;596:5415–28.
72. Brown RW, Peterson DJ. Applications of the neonatal quinpirole model to psychosis and convergence upon the dopamine D(2) receptor. *Curr Top Behav Neurosci.* 2016;29:387–402.
73. Bono F, Savoia P, Guglielmi A, Gennarelli M, Piovani G, Sigala S, et al. Role of dopamine D2/D3 receptors in development, plasticity, and neuroprotection in human iPSC-derived midbrain dopaminergic neurons. *Mol Neurobiol.* 2018;55:1054–67.
74. Shao W, Zhang SZ, Tang M, Zhang XH, Zhou Z, Yin YQ, et al. Suppression of neuroinflammation by astrocytic dopamine D2 receptors via α B-crystallin. *Nature.* 2013;494:90–4.
75. Gu XT, Liu L, Shen Q, Xing D. Photoactivation of ERK/CREB/VMAT2 pathway attenuates MPP(+)-induced neuronal injury in a cellular model of Parkinson's disease. *Cell Signal.* 2017;37:103–14.
76. Fon EA, Pothos EN, Sun BC, Killeen N, Sulzer D, Edwards RH. Vesicular transport regulates monoamine storage and release but is not essential for amphetamine action. *Neuron.* 1997;19:1271–83.
77. Eiden LE, Weihe E. VMAT2: a dynamic regulator of brain monoaminergic neuronal function interacting with drugs of abuse. *Ann N Y Acad Sci.* 2011;1216:86–98.
78. Erickson JD, Eiden LE, Hoffman BJ. Expression cloning of a reserpine-sensitive vesicular monoamine transporter. *Proc Natl Acad Sci USA.* 1992;89:10993–7.
79. Liu Y, Peter D, Roghani A, Schuldiner S, Privé GG, Eisenberg D, et al. A cDNA that suppresses MPP+ toxicity encodes a vesicular amine transporter. *Cell.* 1992;70:539–51.
80. Carlsson T, Björklund T, Kirik D. Restoration of the striatal dopamine synthesis for Parkinson's disease: viral vector-mediated enzyme replacement strategy. *Curr Gene Ther.* 2007;7:109–20.
81. Cersosimo MG, Raina GB, Pecci C, Pellene A, Calandra CR, Gutiérrez C, et al. Gastrointestinal manifestations in Parkinson's disease: prevalence and occurrence before motor symptoms. *J Neurol.* 2013;260:1332–8.
82. Nahmani M, Erisir A. VGlut2 immunohistochemistry identifies thalamocortical terminals in layer 4 of adult and developing visual cortex. *J Comp Neurol.* 2005;484:458–73.
83. Zhou ZD, Saw WT, Ho PGH, Zhang ZW, Zeng L, Chang YY, et al. The role of tyrosine hydroxylase-dopamine pathway in Parkinson's disease pathogenesis. *Cell Mol Life Sci.* 2022;79:599.
84. Jia FJ, Song N, Wang WW, Du XX, Chi YJ, Jiang H. High dietary iron supplement induces the nigrostriatal dopaminergic neurons lesion in transgenic mice expressing mutant A53T human alpha-synuclein. *Front Aging Neurosci.* 2018;10:97.
85. Bhattarai Y, Si J, Pu M, Ross OA, McLean PJ, Till L, et al. Role of gut microbiota in regulating gastrointestinal dysfunction and motor symptoms in a mouse model of Parkinson's disease. *Gut Microbes.* 2021;13:1866974.
86. Haavik J, Toska K. Tyrosine hydroxylase and Parkinson's disease. *Mol Neurobiol.* 1998;16:285–309.
87. Jiao S, Gurevich V, Wolff JA. Long-term correction of rat model of Parkinson's disease by gene therapy. *Nature.* 1996;380:734.
88. Kang UJ, Lee WY, Chang JW. Gene therapy for Parkinson's disease: determining the genes necessary for optimal dopamine replacement in rat models. *Hum Cell.* 2001;14:39–48.
89. Doring MJ, Naegel JR, O'Malley KL, Geller AI. Long-term behavioral recovery in parkinsonian rats by an HSV vector expressing tyrosine hydroxylase. *Science.* 1994;266:1399–403.
90. Steven A, Friedrich M, Jank P, Heimer N, Budczies J, Denkert C, et al. What turns CREB on? And off? And why does it matter? *Cell Mol Life Sci.* 2020;77:4049–67.
91. Zhang C, Zhu PH, Zhang MY, Huang ZC, Hippolyte AR, Hou Y, et al. Identification, classification and characterization of LBD transcription factor family genes in pinus massoniana. *Int J Mol Sci.* 2022;23:13215.
92. Hartzell DD, Trinklein ND, Mendez J, Murphy N, Aldred SF, Wood K, et al. A functional analysis of the CREB signaling pathway using HaloCHIP-chip and high throughput reporter assays. *BMC Genomics.* 2009;10:497.



Open Access This article is licensed under a Creative Commons Attribution 4.0 International License, which permits use, sharing, adaptation, distribution and reproduction in any medium or format, as long as you give appropriate credit to the original author(s) and the source, provide a link to the Creative Commons license, and indicate if changes were made. The images or other third party material in this article are included in the article's Creative Commons license, unless indicated otherwise in a credit line to the material. If material is not included in the article's Creative Commons license and your intended use is not permitted by statutory regulation or exceeds the permitted use, you will need to obtain permission directly from the copyright holder. To view a copy of this license, visit <http://creativecommons.org/licenses/by/4.0/>.

© The Author(s) 2023